

# Robust path following for autonomous vehicles with spatial PH quintic splines

Vincenzo Calabrò<sup>[0000–0003–1246–3128]</sup>

Carlotta Giannelli<sup>[0000–0002–5137–1405]</sup>

Lorenzo Sacco<sup>[0000–0003–2458–5421]</sup>

Alessandra Sestini<sup>[0000–0003–4871–1453]</sup>

**Abstract** The distinctive feature of a polynomial parametric speed let polynomial Pythagorean-hodograph (PH) curves be attractive for the design of accurate and efficient application algorithms. We propose a robust path following scheme for the construction of smooth spatial motions by exploiting PH spline curves. In order to cover a general configuration setting, we present a guidance law which is suitable both for fully-actuated and (more common) under-actuated vehicles, which cannot control all the degrees of freedom. The robustness of the guidance law is enhanced by also taking into account the influence of wind or currents into the equations of motion. A selection of numerical experiments validates the effectiveness of the control strategy when  $C^1$  spatial PH quintic interpolants are suitably considered for both kinematic and dynamic simulations.

## 1 Introduction

In different application frameworks, from the design of suitable paths for unmanned aerial vehicles (UAVs) or autonomous underwater vehicles (AUVs) to algorithms for computer numerical control machines, a path planning strategy should provide an optimal trade-off between the accuracy of the prescribed trajectory, the efficiency of the control algorithms, and the flexibility of the orientation control of a moving rigid body. To design efficient techniques, the accuracy and the versatility of the motion are usually pe-

---

Vincenzo Calabrò

MDM Team S.r.l, Florence, Italy e-mail: [vincenzo.calabro@mdmteam.eu](mailto:vincenzo.calabro@mdmteam.eu)

C. Giannelli, L. Sacco, and A. Sestini

Dipartimento di Matematica e Informatica “Ulisse Dini”, Università degli Studi di Firenze, Florence, Italy e-mail: [carlotta.giannelli@unifi.it](mailto:carlotta.giannelli@unifi.it), [lorenzo.sacco@unifi.it](mailto:lorenzo.sacco@unifi.it), [alessandra.sestini@unifi.it](mailto:alessandra.sestini@unifi.it)

nalized by approximation schemes based on simple curve types (e.g., linear or circular segments). This kind of restriction can be overcome by considering Pythagorean-hodograph (PH) curves, see [6, 10] and references therein, characterized by the distinctive feature of a polynomial parametric speed. Algorithms based on PH curve constructions allow to consider smooth spline paths suitable for real-time applications and robust arrival time estimations. Efficient techniques for time computation are crucial in several applications, as the coordinated arrival of vehicle swarms [9, 15] and the logistical management of different kind of vehicles [20, 26].

In this work we focus on marine robotics, see e.g. [12]. The model typically used to simulate submerged AUVs kinematics has six degrees of freedom and is generally associated with two ordinary differential equations (ODEs). First, it is necessary to define two reference frames: the *navigation* reference frame, an inertial frame with a fixed origin, and the *body-fixed* reference frame, whose origin is fixed on a point of the vehicle, while the axes are integral with its movements. By using the quaternion algebra<sup>1</sup>, the first equation of the considered kinematic model is an ordinary differential equation (ODE) in  $\mathbb{R}^3$  which expresses the change  $\dot{\boldsymbol{\eta}}$  of body position in the navigation reference system through a rotation defined by the unit quaternion  $\boldsymbol{Q} = \boldsymbol{Q}(t)$  as

$$\dot{\boldsymbol{\eta}} = \boldsymbol{Q} \boldsymbol{v}_r^b \boldsymbol{Q}^* + \dot{\boldsymbol{\eta}}_c, \quad (1)$$

where  $\boldsymbol{v}_r^b = (u_r^b, v_r^b, w_r^b)^\top$  is the velocity of the vehicle with respect to the body-fixed reference frame and  $\dot{\boldsymbol{\eta}}_c \in \mathbb{R}^3$  is a constant drift velocity of the fluid [13]. The second equation of the model is an ODE in the quaternion algebra specifying the change of body orientation,

$$\dot{\boldsymbol{Q}} = \frac{1}{2} \boldsymbol{\omega} \boldsymbol{Q} = \frac{1}{2} \boldsymbol{Q} \boldsymbol{\omega}^b, \quad (2)$$

where  $\boldsymbol{\omega}$  is the angular velocity vector of the body in the navigation reference system and  $\boldsymbol{\omega}^b = \boldsymbol{Q}^* \boldsymbol{\omega} \boldsymbol{Q}$  gives its representation in the body-fixed frame.

Guidance, navigation, and control are three fundamental parts in the design of control systems for autonomous or unmanned vehicles. In particular, the guidance module is responsible of providing kinematics reference to be followed. In this paper, we focus on the guidance module [3], considering a *path following* approach, see, e.g., [19]. In this case a software module is responsible of generating a suitable velocity profile  $\dot{\boldsymbol{\eta}}_d$  to be followed so that the vehicle moves along a desired geometric path without any particular time constraint. As our goal is to use the autonomous vehicles in presence of unknown external disturbance, we aim at choosing path following for its intrinsic capability of dealing with these scenarios. We present a guidance law which is suitable both for fully-actuated and (more common) under-actuated vehicles, which cannot control all the degrees of freedom.

---

<sup>1</sup> In this paper we follow the quaternion notation considered in [6, 10].

The structure of the paper is as follows. Section 2 briefly introduces Pythagorean-hodograph spline curves, while Section 3 and Section 4 present the basic and the extended versions of the guidance law, respectively. Kinematic and dynamic simulations are then introduced and commented in Section 5. Finally, Section 6 concludes the paper.

## 2 Spatial PH interpolating spline paths

We want to construct a  $C^1$  smooth spatial spline path  $\boldsymbol{\eta}_p(u)$  that interpolates a given ordered set of points  $\mathbf{p}_k \in \mathbb{E}^3, k = 0, \dots, N$ , and corresponding tangent vectors  $\mathbf{d}_0, \dots, \mathbf{d}_N$  (first order Hermite interpolation) so that

$$\boldsymbol{\eta}_p(u_k) = \mathbf{p}_k, \quad \boldsymbol{\eta}'_p(u_k) = \mathbf{d}_k, \quad k = 0, \dots, N,$$

for a certain choice of parameter values  $u_0, \dots, u_N$ , with  $u_0 < u_1 < \dots < u_N$ . Different schemes for associating appropriate interpolation parameters, see, e.g., [5], and suitable tangent vectors, see, e.g., [1, 18], to the given points sequence can be considered. Besides these interpolation conditions, we require that each spline segment  $\boldsymbol{\eta}_{p,k}$  that defines the spline path,

$$\boldsymbol{\eta}_p(u) := \boldsymbol{\eta}_{p,k}(u) = (x_k(u), y_k(u), z_k(u))^\top \text{ if } u \in [u_{k-1}, u_k]$$

for  $k = 1, \dots, N$ , is a polynomial Pythagorean-hodograph (PH) curve, see [6] and references therein. This means that each hodograph segment  $\boldsymbol{\eta}'_{p,k}(u) = (x'_k(u), y'_k(u), z'_k(u))^T$  has to satisfy the Pythagorean condition

$$x'_k{}^2(u) + y'_k{}^2(u) + z'_k{}^2(u) = \sigma_k^2(u),$$

for some polynomial  $\sigma_k$  that represents the curve parametric speed, i.e.  $\sigma_k(u) = \|\boldsymbol{\eta}'_{p,k}(u)\| = ds/du$ , where  $s$  is the cumulative arc length and  $\|\cdot\|$  denotes the standard Euclidean norm.

Spatial PH curves admit a compact representation using the algebra of quaternions and Bernstein polynomials  $b_i^n(\xi) := \binom{n}{i} \xi^i (1 - \xi)^{n-i}$ ,  $\xi \in [0, 1]$ , for  $i = 0, \dots, n$ . By focusing on the quintic case, the hodograph segment  $\boldsymbol{\eta}'_{p,k}$  can be expressed as a quaternion product of the form

$$\boldsymbol{\eta}'_{p,k}(u) = \mathcal{A}_k(u) \mathbf{w} \mathcal{A}_k^*(u), \quad (3)$$

where  $\mathbf{w}$  is any fixed unit vector and  $\mathcal{A}_k(u)$  is a quadratic quaternion polynomial which can be expressed in standard Bézier form as

$$\mathcal{A}_k(u) := \sum_{i=0}^2 \mathcal{A}_{k,i} b_i^2 \left( \frac{u - u_{k-1}}{h_k} \right),$$

with  $\mathcal{A}_{k,i} \in \mathbb{H}$ , for  $i = 0, 1, 2$  and  $h_k := u_k - u_{k-1}$ . By integrating the hodograph (3), we obtain the  $k$ -th spline segment:

$$\boldsymbol{\eta}_{p,k}(u) = \sum_{i=0}^5 \mathbf{q}_{k,i} b_i^5 \left( \frac{u - u_{k-1}}{h_k} \right), \quad u \in [u_{k-1}, u_k],$$

defined in terms of the Bézier control points

$$\begin{aligned} \mathbf{q}_{k,1} &= \mathbf{q}_{k,0} + \frac{h_k}{5} \mathcal{A}_{k,0} \mathbf{w} \mathcal{A}_{k,0}^*, \quad \mathbf{q}_{k,2} = \mathbf{q}_{k,1} + \frac{h_k}{10} (\mathcal{A}_{k,0} \mathbf{w} \mathcal{A}_{k,1}^* + \mathcal{A}_{k,1} \mathbf{w} \mathcal{A}_{k,0}^*), \\ \mathbf{q}_{k,3} &= \mathbf{q}_{k,2} + \frac{h_k}{30} (\mathcal{A}_{k,0} \mathbf{w} \mathcal{A}_{k,2}^* + 4 \mathcal{A}_{k,1} \mathbf{w} \mathcal{A}_{k,1}^* + \mathcal{A}_{k,2} \mathbf{w} \mathcal{A}_{k,0}^*), \\ \mathbf{q}_{k,4} &= \mathbf{q}_{k,3} + \frac{h_k}{10} (\mathcal{A}_{k,1} \mathbf{w} \mathcal{A}_{k,2}^* + \mathcal{A}_{k,2} \mathbf{w} \mathcal{A}_{k,1}^*), \quad \mathbf{q}_{k,5} = \mathbf{q}_{k,4} + \frac{h_k}{5} \mathcal{A}_{k,2} \mathbf{w} \mathcal{A}_{k,2}^*, \end{aligned}$$

with  $\mathbf{q}_{k,0} = \mathbf{p}_{k-1}$ . In each spline segment, for  $u \in [u_{k-1}, u_k]$ , the parametric speed is a quartic polynomial  $\sigma_k(u) = \mathcal{A}_k(u) \mathcal{A}_k(u)^*$ . The distinctive polynomial form of the parametric speed  $\sigma$  that characterizes the family of spatial PH curves enables an *exact* and *efficient* computation of the curve arc length, which can be obtained without numerical quadrature by a finite sequence of arithmetic operations on the Bézier coefficients. This key feature is strictly connected to the availability of a real-time estimation of the vehicle arrival time. As a matter of fact, it is always possible to compute a first raw estimation of this quantity, starting from the cruise speed and the analytic evaluation of the length of the trajectory. Many papers recently addressed different application problems with planar or spatial PH curves for the control of autonomous vehicles, see, e.g., [9] and references therein. In the planar case, PH splines have also been considered in connection with obstacle avoidance techniques [4, 16] and to test a  $C^2$  feedrate scheduling algorithm [17].

We observe that the problem of first order Hermite interpolation by spatial PH quintics admits a two-parameter family of formal solutions [7, 25]. In this paper we consider the CC criterion introduced in [8] in view of its computational simplicity and of the high shape quality of the interpolants it yields. Note that the approximation order of the interpolation scheme based on this criterion was analyzed in [22].

### 3 Guidance law

As stated in Section 1, the goal of a path-following scheme is to prescribe the vehicle velocity commands needed to achieve motion control objectives [3]. This goal is generally achieved by means of a guidance law capable of combining both navigation information, such as vehicle position, with desired

path geometrical information, such as tangent direction, parameter value, etc. We will now detail the path parameterization and the base guidance law derived from [2].

### 3.1 Path parameterization

Let us consider a vehicle described in a navigation reference frame. Being the vehicle a rigid body, its position at a certain time instant  $t$  can be described by the position  $\boldsymbol{\eta}(t) = (x(t), y(t), z(t))^T \in \mathbb{E}^3$  of one of its points. Concerning the geometric path, we adopt the PH spline parametric representation introduced in the previous section,  $\boldsymbol{\eta}_p(u) = (x_p(u), y_p(u), z_p(u))^T \in \mathbb{E}^3$ ,  $u \in [u_0, u_N]$ . Note that, since only first order derivatives are involved in the calculation of relevant guidance law parts,  $\boldsymbol{\eta}_p$  is required to be  $C^1$  smooth and this motivates our choice of spatial  $C^1$  PH spline paths.

We introduce an adapted reference path frame  $(\mathbf{i}_p, \mathbf{j}_p, \mathbf{k}_p)$ , with vertex at  $\mathbf{p}_p(u)$  and with the  $x$ -axis (aligned with  $\mathbf{i}_p$ ) directed as the tangent to the curve. Since additional requirements on the adapted frame are not considered, the unit quaternion  $\mathcal{Q}_p$  which maps vectors represented in the path reference system to the navigation one, is just required to satisfy the following vector equation (expressed in quaternion algebra):

$$\mathcal{Q}_p(1, 0, 0)^T \mathcal{Q}_p^* = \frac{\boldsymbol{\eta}'_p}{\|\boldsymbol{\eta}'_p\|}, \quad (4)$$

where standard Euclidean norm is considered. We can then define  $\mathcal{Q}_p$  in terms of only two angles (instead of three). In particular, following [2], we set

$$\mathcal{Q}_p = \mathcal{Q}_z(\chi_p) \mathcal{Q}_y(\nu_p), \quad (5)$$

where  $\mathcal{Q}_z(\chi_p)$  and  $\mathcal{Q}_y(\nu_p)$  are the two unit quaternions

$$\mathcal{Q}_z(\chi_p) := \left( \cos \frac{\chi_p}{2}, 0, 0, \sin \frac{\chi_p}{2} \right)^T, \quad \mathcal{Q}_y(\nu_p) := \left( \cos \frac{\nu_p}{2}, 0, \sin \frac{\nu_p}{2}, 0 \right)^T,$$

which define a rotation of an angle  $\chi_p$  (*azimuth* angle) and  $\nu_p$  (*elevation* angle) about the  $z$  and the  $y$  axes, respectively. With the help of quaternion algebra, it can be easily shown that, in order to satisfy (4), the azimuth and elevation angles have to be defined as

$$\chi_p(u) = \mathbf{atan}_2(x'_p(u), y'_p(u)), \quad \nu_p(u) = \mathbf{atan}_2(-z'_p(u), \sqrt{x'_p(u)^2 + y'_p(u)^2}),$$

where  $\mathbf{atan}_2$  denotes the four quadrant inverse tangent. By following the literature in the field, to evaluate the performances of our path following scheme, in our numerical experiments we consider the track error

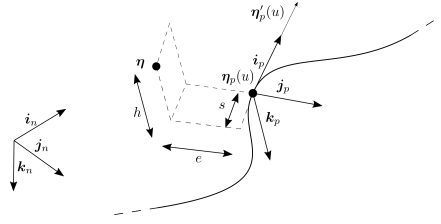


**Fig. 1** Navigation frame (left), path reference frame and track errors  $s, e, h$  (right).

$$\boldsymbol{\epsilon}^p = (s, e, h)^\top := \mathcal{Q}_p^*(\boldsymbol{\eta} - \boldsymbol{\eta}_p(u))\mathcal{Q}_p, \quad (6)$$

which is the expression of the error vector  $(\boldsymbol{\eta} - \boldsymbol{\eta}_p(u))$  in the path reference system. The Cartesian components  $s, e, h$  of the track error are usually called *along-track* error, *cross-track* error, and *vertical-track* error, respectively. The path reference frame  $(\boldsymbol{i}_p, \boldsymbol{j}_p, \boldsymbol{k}_p)$  and the error components  $s, e, h$  are depicted in Fig. 1, together with the navigation frame  $(\boldsymbol{i}_n, \boldsymbol{j}_n, \boldsymbol{k}_n)$ .

### 3.2 Guidance law

The objective of the guidance control law is to ensure the convergence of the vehicle to the geometric path. This is done by generating a function  $u = u(t)$  and a suitable desired velocity  $\dot{\boldsymbol{\eta}}_d(t) = (\dot{x}_d(t), \dot{y}_d(t), \dot{z}_d(t))^\top \in \mathbb{R}^3$  so that

$$\lim_{t \rightarrow +\infty} \|\boldsymbol{\eta}(t) - \boldsymbol{\eta}_p(u(t))\| = 0, \quad (7)$$

where we assume that the vehicle can have at each time instant the desired velocity, and consequently  $\dot{\boldsymbol{\eta}} = \dot{\boldsymbol{\eta}}_d$ . We then consider an additional reference frame attached to the vehicle for the development of the guidance law proposed in [2], which is here revisited. This frame is called *desired reference frame*, since its  $x$ -axis is in the direction of the desired velocity. Conversely, the representation of the desired velocity in this frame is  $(U_d, 0, 0)^\top$ , where  $U_d := \|\dot{\boldsymbol{\eta}}_d\|$  is the desired vehicle speed. A corresponding unit quaternion  $\mathcal{Q}_d$  is then necessary to represent the desired velocity in the navigation reference system,  $\dot{\boldsymbol{\eta}}_d := \mathcal{Q}_d(U_d, 0, 0)^\top \mathcal{Q}_d^*$ . Thus, analogously to  $\mathcal{Q}_p$  which was defined through (5), also  $\mathcal{Q}_d$  can be defined as the product of two unit quaternions  $\mathcal{Q}_{d,z}(\chi_d)$  and  $\mathcal{Q}_{d,y}(\nu_d)$ , using just two angles  $\chi_d$  and  $\nu_d$ . In [2] it was shown that a suitable choice for these angles is

$$\chi_d = \arctan\left(\frac{x_{num}}{x_{den}}\right), \quad \nu_d = \arcsin(\sin \nu_p \cos \chi_r \cos \nu_r + \cos \nu_p \sin \nu_r), \quad (8)$$

with

$$\begin{aligned} x_{num} &= \cos \chi_p \sin \chi_r \cos \nu_r - \sin \chi_p \sin \nu_p \sin \nu_r + \sin \chi_p \cos \chi_r \cos \nu_p \cos \nu_r, \\ x_{den} &= -\sin \chi_p \sin \chi_r \cos \nu_r - \cos \chi_p \sin \nu_p \sin \nu_r + \cos \chi_p \cos \chi_r \cos \nu_p \cos \nu_r, \end{aligned}$$

$$\chi_r(e) = \arctan \left( -\frac{e}{\Delta_e} \right), \quad \nu_r(h) = \arctan \left( \frac{h}{\Delta_h} \right), \quad (9)$$

where  $\Delta_h = \mu \sqrt{\Delta_e^2 + e^2}$ , while  $\Delta_e$  and  $\mu$  are two positive guidance parameters. For fixed values of  $e$  and  $h$  in (6), the guidance parameters  $\Delta_e$  and  $\mu$  influence the direction of convergence along the azimuth and elevation plane respectively. By taking into account (8) and (9), let us consider  $\dot{u} := (U_d \cos \chi_r \cos \nu_r + \gamma s) / \|\boldsymbol{\eta}'_p\|$ , where  $\gamma$  is another positive control parameter influencing the convergence of the along-track error  $s$ . For this choice, the Lyapunov theory related to the stability of non linear Cauchy problems ensures that an equilibrium solution  $\boldsymbol{\epsilon}^p = \mathbf{0}$  is obtained for any positive  $U_d$  and control parameters [2]. In particular, if

$$U_d = \frac{U_0}{\mu \Delta_e} \sqrt{\mu^2 (\Delta_e^2 + e^2) + h^2}, \quad (10)$$

where  $U_0$  is a given positive constant velocity value, then uniform global exponential stability (UGES) can be achieved, see [24]. Now, when the vehicle converges to the path,  $U_d$  tends to  $U_0$ . Consequently, the value  $U_0$  can be considered a desired speed at steady state. In general, the choice of a suitable value for this steady speed is delegated to the operator.

Note that, in practice, the vehicle will not be able to keep the prescribed velocity, since in the fluid there is a current that can be modelled as a velocity vector  $\dot{\boldsymbol{\eta}}_c$ . By denoting with  $\dot{\boldsymbol{\eta}}_r$  the velocity of the vehicle relative to the fluid, in order to consider a more realistic velocity for the vehicle, since  $\dot{\boldsymbol{\eta}} = \dot{\boldsymbol{\eta}}_r + \dot{\boldsymbol{\eta}}_c$ , we should assume  $\dot{\boldsymbol{\eta}}_r = \dot{\boldsymbol{\eta}}_d$ . Our experiments clearly confirm that this choice does not guarantee the convergence of  $\boldsymbol{\eta}$  to the path, even under the assumption of a moderate constant current velocity,<sup>2</sup> see for example the center plots in Fig. 2. In the next section we will introduce a new relative desired velocity  $\dot{\boldsymbol{\eta}}_{rd}$  to recover the right vehicle behaviour even when a current drifting  $\dot{\boldsymbol{\eta}}_c$  is considered.

## 4 Extended guidance law

In this section we will present an extended version of the basic guidance law to handle two major improvements: (1) derive a suitable estimation of the ocean current to be effective in realistic scenarios, see Section 4.1, and (2) provide the desired velocity in a suitable form for general under-actuated

---

<sup>2</sup> The hypothesis of a constant current is a common assumption in the literature, since it is reasonable during not very long time periods.

underwater vehicles with limited actuation capabilities (i.e., torpedo-like), see Section 4.2. These vehicles are typically designed to exploit longitudinal speed at cost of reduced maneuverability. This reflects the limited control possibilities, dealing typically with a single main propeller coupled with a pair of rudders. A simple, yet effective, configuration of this kind reduces the available degrees of freedom of the vehicle to the *surge motion*, used mainly for longitudinal propulsion, the *pitch rotation*, used to steer the vehicle nose up and down to change depth and the *yaw rotation*, used to steer the vehicle nose left and right to change its planar position. For this reason, it is necessary to provide to the controller a desired velocity triplet  $(u_{rd}^b, \omega_{yd}^b, \omega_{zd}^b)$ , where  $u_{rd}^b$  is the surge velocity over the  $x$ -axis of the body-fixed frame,  $\omega_{yd}^b$  is the pitch angular velocity about the  $y$ -axis of the body-fixed frame and  $\omega_{zd}^b$  is the yaw angular velocity about the  $z$ -axis of the body-fixed frame.

#### 4.1 Estimation of kinematic drifts

We will now consider the presence of a current, modelled as a velocity vector of the fluid  $\dot{\boldsymbol{\eta}}_c$ . With this hypothesis, the velocity of the vehicle can not reach the desired value, since it is only possible to assign the relative desired velocity  $\dot{\boldsymbol{\eta}}_{rd}$  and

$$\dot{\boldsymbol{\eta}} = \dot{\boldsymbol{\eta}}_{rd} + \dot{\boldsymbol{\eta}}_c, \quad (11)$$

where  $\dot{\boldsymbol{\eta}}_{rd} = \dot{\boldsymbol{\eta}}_r$ . For this reason, a suitable estimation of the current drift is needed. Let  $\hat{\dot{\boldsymbol{\eta}}}_c$  be the estimated velocity of the current. By considering the new relative desired velocity as  $\dot{\boldsymbol{\eta}}_{rd} = \dot{\boldsymbol{\eta}}_d - \hat{\dot{\boldsymbol{\eta}}}_c$  in (11), we obtain

$$\dot{\boldsymbol{\eta}} = \dot{\boldsymbol{\eta}}_d - \hat{\dot{\boldsymbol{\eta}}}_c + \dot{\boldsymbol{\eta}}_c. \quad (12)$$

If the estimate of the current tends to its real value, it is clear that we come back to  $\dot{\boldsymbol{\eta}} = \dot{\boldsymbol{\eta}}_d$ . As a consequence, all the convergence results presented in Section 3 still hold true. In the following theorem we derive a suitable estimation for the (constant) current drift that guarantees (7).

**Theorem 1.** *Let the fluid have constant irrotational current  $\dot{\boldsymbol{\eta}}_c$  and  $\dot{\boldsymbol{\eta}}$  given by (12). If  $\hat{\dot{\boldsymbol{\eta}}}_d$  is computed with the guidance law of Section 3 and*

$$\ddot{\hat{\boldsymbol{\eta}}}_c = k_c(\boldsymbol{\eta} - \boldsymbol{\eta}_p), \quad \text{with } k_c > 0, \quad (13)$$

*then  $\lim_{t \rightarrow \infty} \|\dot{\hat{\boldsymbol{\eta}}}_c\| = 0$  and  $\lim_{t \rightarrow \infty} \|\boldsymbol{\epsilon}^p\| = 0$ , where  $\dot{\hat{\boldsymbol{\eta}}}_c := \dot{\boldsymbol{\eta}}_c - \dot{\hat{\boldsymbol{\eta}}}_c$  is the estimation error and  $\boldsymbol{\epsilon}^p$  is the track error.*

**Proof :** The modified dynamical system representing the new path following strategy is characterized by the state vector  $\boldsymbol{\epsilon}^p$  defined in (6) and by  $\dot{\hat{\boldsymbol{\eta}}}_c \in \mathbb{R}^3$ . We want to demonstrate that the system admits the asymptotically stable equilibrium solution  $(\boldsymbol{\epsilon}^p, \dot{\hat{\boldsymbol{\eta}}}_c)^\top = (\mathbf{0}, \mathbf{0})^\top$ . It is trivial to demonstrate that the



vanishing of  $\boldsymbol{\epsilon}^p$  and  $\dot{\check{\boldsymbol{\eta}}}_c$  leads to  $\dot{\boldsymbol{\epsilon}}^p = \mathbf{0}$  and  $\ddot{\check{\boldsymbol{\eta}}}_c = \mathbf{0}$ , implying that the solution is an equilibrium. For the stability analysis of such equilibrium solution, let us consider the following Lyapunov function:  $V(\boldsymbol{\epsilon}^p, \dot{\check{\boldsymbol{\eta}}}_c) := k_c \frac{1}{2} \boldsymbol{\epsilon}^{p\top} \boldsymbol{\epsilon}^p + \frac{1}{2} \dot{\check{\boldsymbol{\eta}}}_c^\top \dot{\check{\boldsymbol{\eta}}}_c$ . It holds that  $V(\boldsymbol{\epsilon}^p, \dot{\check{\boldsymbol{\eta}}}_c) \geq 0$ , with  $V(\boldsymbol{\epsilon}^p, \dot{\check{\boldsymbol{\eta}}}_c) = 0$  if and only if  $\boldsymbol{\epsilon}^p = \dot{\check{\boldsymbol{\eta}}}_c = \mathbf{0}$ . In order to study the behavior of this function, we need now to compute its time derivative

$$\dot{V}(\boldsymbol{\epsilon}^p, \dot{\check{\boldsymbol{\eta}}}_c) = k_c \boldsymbol{\epsilon}^{p\top} \dot{\boldsymbol{\epsilon}}^p + \dot{\check{\boldsymbol{\eta}}}_c^\top \ddot{\check{\boldsymbol{\eta}}}_c. \quad (14)$$

By considering the definition of  $\boldsymbol{\epsilon}^p$  in (6), together with (12), we obtain

$$\begin{aligned} \dot{\boldsymbol{\epsilon}}^p &= \dot{Q}_p^*(\boldsymbol{\eta} - \boldsymbol{\eta}_p(u)) \mathcal{Q}_p + Q_p^*(\boldsymbol{\eta} - \boldsymbol{\eta}_p(u)) \dot{Q}_p + Q_p^*(\dot{\boldsymbol{\eta}} - \dot{\boldsymbol{\eta}}_p(u)) \mathcal{Q}_p \\ &= \dot{Q}_p^* \mathcal{Q}_p \boldsymbol{\epsilon}^p + \boldsymbol{\epsilon}^p Q_p^* \dot{Q}_p + Q_p^*(\dot{\boldsymbol{\eta}}_d + \dot{\check{\boldsymbol{\eta}}}_c - \boldsymbol{\eta}'_p \dot{u}) \mathcal{Q}_p. \end{aligned} \quad (15)$$

Furthermore, since a constant current implies  $\ddot{\check{\boldsymbol{\eta}}}_c = \mathbf{0}$ , we have that  $\ddot{\check{\boldsymbol{\eta}}}_c = -\ddot{\check{\boldsymbol{\eta}}}_c$ . Replacing the derived expressions of  $\dot{\boldsymbol{\epsilon}}^p$  and of  $\ddot{\check{\boldsymbol{\eta}}}_c$  into (14), we obtain

$$\begin{aligned} \dot{V}(\boldsymbol{\epsilon}^p, \dot{\check{\boldsymbol{\eta}}}_c) &= k_c \boldsymbol{\epsilon}^{p\top} (\dot{Q}_p^* \mathcal{Q}_p \boldsymbol{\epsilon}^p + \boldsymbol{\epsilon}^p Q_p^* \dot{Q}_p + Q_p^*(\dot{\boldsymbol{\eta}}_d + \dot{\check{\boldsymbol{\eta}}}_c - \boldsymbol{\eta}'_p \dot{u}) \mathcal{Q}_p) + \dot{\check{\boldsymbol{\eta}}}_c^\top (-\ddot{\check{\boldsymbol{\eta}}}_c) \\ &= k_c \dot{V}_e(\boldsymbol{\epsilon}^p) + \dot{V}_c(\boldsymbol{\epsilon}^p, \dot{\check{\boldsymbol{\eta}}}_c), \end{aligned}$$

where  $\dot{V}_e(\boldsymbol{\epsilon}^p) := \boldsymbol{\epsilon}^{p\top} (\dot{Q}_p^* \mathcal{Q}_p \boldsymbol{\epsilon}^p + \boldsymbol{\epsilon}^p Q_p^* \dot{Q}_p + Q_p^*(\dot{\boldsymbol{\eta}}_d - \boldsymbol{\eta}'_p \dot{u}) \mathcal{Q}_p)$  is a term corresponding to the same Lyapunov function used in [2], while  $\dot{V}_c(\boldsymbol{\epsilon}^p, \dot{\check{\boldsymbol{\eta}}}_c) := k_c \boldsymbol{\epsilon}^{p\top} (Q_p^* \dot{\check{\boldsymbol{\eta}}}_c \mathcal{Q}_p) - \dot{\check{\boldsymbol{\eta}}}_c^\top (\ddot{\check{\boldsymbol{\eta}}}_c)$  is a new term necessary to study the convergence of the estimation error. For what concern the term  $\dot{V}_e(\boldsymbol{\epsilon}^p)$ , expanding all the products and replacing the values of desired velocity  $\dot{\boldsymbol{\eta}}_c$  and parameter derivative  $\dot{u}$ , after few calculations we have that

$$\dot{V}_e(\boldsymbol{\epsilon}^p) = -\gamma s^2 - \frac{U_0}{\Delta_e} e^2 - \frac{U_0}{\mu \Delta_e} h^2,$$

which is  $\leq 0$  (negative semidefinite) since  $\dot{\check{\boldsymbol{\eta}}}_c$  could be non-zero when  $\dot{V}_e(\boldsymbol{\epsilon}^p) = 0$ . Let us now verify that the term  $\dot{V}_c(\boldsymbol{\epsilon}^p, \dot{\check{\boldsymbol{\eta}}}_c)$  vanishes. Since  $\ddot{\check{\boldsymbol{\eta}}}_c = k_c(\boldsymbol{\eta} - \boldsymbol{\eta}_p)$ , we obtain  $\dot{V}_c(\boldsymbol{\epsilon}^p, \dot{\check{\boldsymbol{\eta}}}_c) = k_c(\boldsymbol{\epsilon}^{p\top} (Q_p^* \dot{\check{\boldsymbol{\eta}}}_c \mathcal{Q}_p) - \dot{\check{\boldsymbol{\eta}}}_c^\top (Q_p \boldsymbol{\epsilon}^p Q_p^*))$ . The four vectors involved in this equation represent the same two vectors expressed in the path reference frame as  $\boldsymbol{\epsilon}^p$ ,  $Q_p^* \dot{\check{\boldsymbol{\eta}}}_c \mathcal{Q}_p$  and in the navigation reference frame as  $\dot{\check{\boldsymbol{\eta}}}_c$ ,  $Q_p \boldsymbol{\epsilon}^p Q_p^*$  respectively. Consequently,  $\dot{V}_c(\boldsymbol{\epsilon}^p, \dot{\check{\boldsymbol{\eta}}}_c) = 0$  and  $\dot{V}(\boldsymbol{\epsilon}^p, \dot{\check{\boldsymbol{\eta}}}_c) = k_c \dot{V}_e(\boldsymbol{\epsilon}^p) \leq 0$ . We can then conclude that the system is stable. In any case, we need asymptotic stability to have convergence for both current and error estimation. Thus, let us consider the set  $\mathcal{E} = \{(\boldsymbol{\epsilon}^p, \dot{\check{\boldsymbol{\eta}}}_c) \mid \dot{V}(\boldsymbol{\epsilon}^p, \dot{\check{\boldsymbol{\eta}}}_c) = 0\} = \{(\boldsymbol{\epsilon}^p, \dot{\check{\boldsymbol{\eta}}}_c) \mid \boldsymbol{\epsilon}^p = \mathbf{0}\}$ . We can observe that  $\mathcal{E}$  does not contain any trajectory of the system, except the equilibrium solution  $\boldsymbol{\epsilon}^p = \dot{\check{\boldsymbol{\eta}}}_c = \mathbf{0}$ . Indeed, if we had  $\boldsymbol{\epsilon}^p = \mathbf{0}$  but  $\dot{\check{\boldsymbol{\eta}}}_c \neq \mathbf{0}$ , replacing inside (15) it would result that  $\dot{\boldsymbol{\epsilon}}^p \neq \mathbf{0}$ , and so the trajectory would not stay inside  $\mathcal{E}$ . As a result we can conclude that the system is asymptotically stable by applying the *LaSalle-Krasovskii principle*, see e.g. [23]. ■

## 4.2 Mapping desired guidance into controllable axes

The result of Theorem 1 allows the vehicle to reject errors caused by the presence of a current but the desired relative velocity  $\dot{\boldsymbol{\eta}}_{rd}$  is a velocity described in the navigation frame. In order to map  $\dot{\boldsymbol{\eta}}_{rd}$  into three body-fixed velocities  $u_{rd}^b, \omega_{yd}^b, \omega_{zd}^b$ , it is necessary to follow the path with a point different from the center of the body-fixed reference frame. We consider for this purpose the head of the vehicle, whose constant position in the body-fixed reference frame is  $\mathbf{O}_h^b = (o_x^b, o_y^b, o_z^b)^\top$ . We can now compute its position  $\boldsymbol{\eta}_h$  in the navigation reference frame as  $\boldsymbol{\eta}_h = \boldsymbol{\eta} + \mathcal{Q} \mathbf{O}_h^b \mathcal{Q}^*$ , where  $\boldsymbol{\eta}$  is the position of the center of the body-fixed reference frame and  $\mathcal{Q}$  is the quaternion representing the attitude of the vehicle. The body-fixed velocity of the head can be computed as  $\mathbf{v}_h^b = \mathcal{Q}^* \dot{\boldsymbol{\eta}}_h \mathcal{Q} = \mathcal{Q}^* (\dot{\boldsymbol{\eta}} + \dot{\mathcal{Q}} \mathbf{O}_h^b \mathcal{Q}^* + \mathcal{Q} \mathbf{O}_h^b \dot{\mathcal{Q}}^*) \mathcal{Q}$ . By substituting the expression for  $\mathcal{Q}$  provided by (2) into the previous equation, while considering that  $\mathcal{Q}$  is a unit quaternion and  $(\boldsymbol{\omega} \mathcal{Q})^* = \mathcal{Q}^* \boldsymbol{\omega}^* = -\mathcal{Q}^* \boldsymbol{\omega}$ , we obtain  $\mathbf{v}_h^b = \mathbf{v}^b + \frac{1}{2} (\boldsymbol{\omega}^b \mathbf{O}_h^b - \mathbf{O}_h^b \boldsymbol{\omega}^b)$ , where we recall that  $\boldsymbol{\omega}^b = \mathcal{Q}^* \boldsymbol{\omega} \mathcal{Q}$ . Thus, using the standard cross product, we can also write  $\mathbf{v}_h^b = \mathbf{v}^b + \boldsymbol{\omega}^b \times \mathbf{O}_h^b = \mathbf{v}^b - \mathbf{O}_h^b \times \boldsymbol{\omega}^b$ . Finally, we can pass to relative velocities:

$$\mathbf{v}_{rh}^b = \mathbf{v}_r^b - \mathbf{O}_h^b \times \boldsymbol{\omega}^b, \quad (16)$$

where  $\mathbf{v}_{rh}^b$  is the relative body-fixed velocity of the head and  $\mathbf{v}_r^b$  is the relative body-fixed velocity of the vehicle. In order to deal with an under-actuated vehicle, we can only control the motion along three directions, as mentioned at the beginning of this section. We can then generate the desired velocities in the following form:

$$\mathbf{v}_{rd}^b = \mathbf{v}_r^b = (u_{rd}^b, 0, 0)^\top, \quad \boldsymbol{\omega}_d^b = \boldsymbol{\omega}^b = (0, \omega_{yd}^b, \omega_{zd}^b)^\top. \quad (17)$$

By substituting  $\mathbf{v}_{rd}^b$  and  $\boldsymbol{\omega}_d^b$  into (16), after some trivial calculations, we obtain:

$$\mathbf{v}_{rhd}^b = \mathbf{v}_{rh}^b = \mathbf{v}_{rd}^b - \mathbf{O}_h^b \times \boldsymbol{\omega}_d^b = \mathbf{P}(\mathbf{O}_h^b) (u_{rd}^b, \omega_{yd}^b, \omega_{zd}^b)^\top, \quad (18)$$

with  $\mathbf{P}(\mathbf{O}_h^b) = (1, o_z^b, -o_y^b; 0, 0, o_x^b; 0, -o_x^b, 0)$ . Since  $\mathbf{O}_h^b$  is the head of the vehicle,  $o_x^b \neq 0$  and, consequently, the matrix  $\mathbf{P}(\mathbf{O}_h^b)$  is invertible. The solution of the linear system in (18) is then  $(u_{rd}^b, \omega_{yd}^b, \omega_{zd}^b)^\top = \mathbf{P}(\mathbf{O}_h^b)^{-1} \mathcal{Q}^* (\dot{\boldsymbol{\eta}}_d - \dot{\boldsymbol{\eta}}_c) \mathcal{Q}$ , where  $\mathbf{v}_{rhd}^b = \mathcal{Q}^* \dot{\boldsymbol{\eta}}_{rd} \mathcal{Q}$  and  $\dot{\boldsymbol{\eta}}_{rd} = (\dot{\boldsymbol{\eta}}_d - \dot{\boldsymbol{\eta}}_c)$ . Summarizing and including the current estimation, the equations of the extended guidance law are

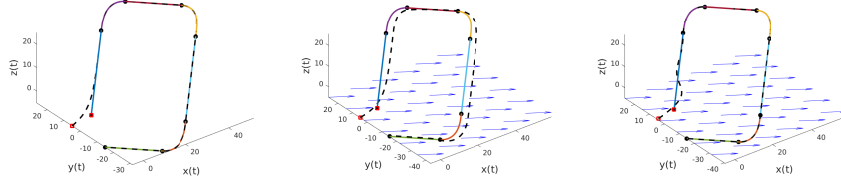


**Fig. 2** Kinematic simulations: results obtained with the guidance law of Section 3 and 4 for the first simulation scenario. The path to be followed (solid line) is shown together with the path of the vehicle (dashed line) in a simulation without current (left) and with current when the basic guidance law (center) or its extension (right) are considered.

$$\begin{aligned}\boldsymbol{\eta}_h &= \boldsymbol{\eta} + \mathcal{Q}\mathcal{O}_h^b\mathcal{Q}^*, & \ddot{\boldsymbol{\eta}}_c &= k_c(\boldsymbol{\eta}_h - \boldsymbol{\eta}_p), \\ (u_{rd}^b, \omega_{yd}^b, \omega_{zd}^b)^\top &= \mathbf{P}(\mathcal{O}_h^b)^{-1}\mathcal{Q}^*(\dot{\boldsymbol{\eta}}_d - \dot{\boldsymbol{\eta}}_c)\mathcal{Q}.\end{aligned}$$

## 5 Numerical tests

For the experiments we consider three different scenarios, performing both kinematic and dynamic simulations to verify the robustness of the scheme. The guidance parameters are set as follows:  $\gamma = 1 \text{ s}^{-1}$ ,  $U_0 = 0.4 \text{ m/s}$ ,  $\Delta_e = 5 \text{ m}$  and  $\mu = 1$  for the base guidance law;  $\mathcal{O}_h^b = (0.8, 0, 0)^\top \text{ m}$  and  $\kappa_c = 0.015 \text{ s}^{-2}$  for the extended guidance law. In all figures related to the paths, the red markers indicate the starting point of the vehicle and the first point of the path. When track errors and current estimation are shown, the vertical dashed lines refer to the junction points of the PH spline path. The black dots indicate the interpolation points.

### 5.1 Kinematic simulations

In the first scenario, the eight points  $\mathbf{p}_0 = (0, 0, 0)^\top$ ,  $\mathbf{p}_1 = (20, 20, 20)^\top$ ,  $\mathbf{p}_2 = (35, 25, 25)^\top$ ,  $\mathbf{p}_3 = (50, 10, 25)^\top$ ,  $\mathbf{p}_4 = (45, -5, 20)^\top$ ,  $\mathbf{p}_5 = (25, -25, 0)^\top$ ,  $\mathbf{p}_6 = (10, -30, -5)^\top$ ,  $\mathbf{p}_7 = (-5, 15, 5)^\top$  are interpolated for the construction of a  $C^1$  PH spline. The tangents in these points are chosen as  $\mathbf{d}_j = \mathbf{d}_{j+1} = (\mathbf{p}_{j+1} - \mathbf{p}_j) / \|\mathbf{p}_{j+1} - \mathbf{p}_j\|$ ,  $j = 0, 2, 4, 6$ . The result is a  $C^1$  PH spline curve composed by seven segments, with total length  $L = 167.0983 \text{ m}$ . By considering as starting point of the vehicle  $\boldsymbol{\eta}(0) = (-5, 5, -5)^\top \text{ m}$ , we test the guidance law (GL) and its extended version (EGL). The drifting current is  $\dot{\boldsymbol{\eta}}_c = (0.15, -0.2, 0.05)^\top \text{ m/s}$ . The results are shown in Fig. 2. The clear shift between the path and the trajectory of the vehicle (center plot in Fig. 2),

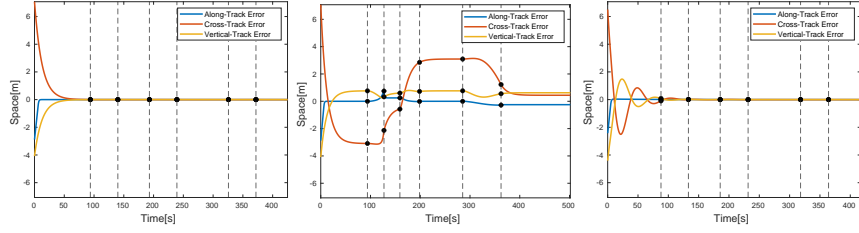


**Fig. 3** Kinematic simulations: track errors obtained with the guidance laws of Section 3 (GL) and 4 (EGL) for the first simulation scenario. The results are shown for a simulation without current (left) and with current when the basic guidance law (center) or its extension (right) are considered.

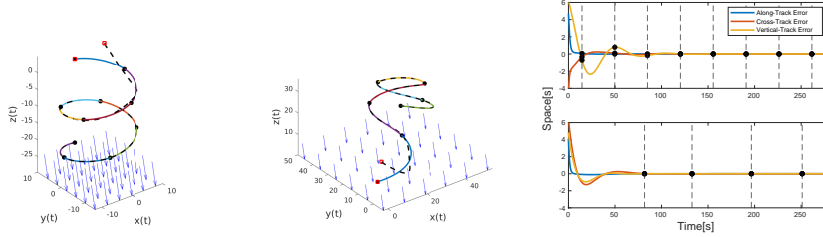


**Fig. 4** Kinematic simulations: results obtained considering the extended guidance laws of Section 4 for the last two scenarios. On the left (second scenario) and on the center (third scenario), the paths to be followed (solid line) are shown together with the paths of the vehicle (dashed line). The track errors obtained for the second (top) and third (bottom) simulation scenario are also shown (right).

exactly in the direction of the current vector, demonstrates that the basic GL is not able to handle current disturbances. This issue is resolved when the EGL is considered (right plot in Fig. 2). Fig. 3 (center) confirms that the error does not converge when the GL is considered in presence of current, since its value depends on the relative direction of the path with respect to the current drift. In Fig. 3 (right) it is also possible to see that, when the EGL is considered, the error converges to zero with just some overshoot effects, as normal consequences of the integral action in the current estimator update. Finally Fig. 5 (left) shows that the current estimation converges to the value of current introduced in the kinematics.

For the second scenario, we sample ten points and derivative vectors from a circular helix of the form  $\mathbf{x}(s) = (a \sin(s/s_0), a \cos(s/s_0), -b(s/s_0))^T$ , with  $s_0 = \sqrt{a^2 + b^2}$ ,  $a = 10$ ,  $b = 2$ , at equidistant parameter values  $s \in [0, n(2\pi s_0)]$ , with  $n = 2$  number of turns. The resulting  $C^1$  PH spline curve with total length  $L = 127.2619$  m, computed with the CC selection criterion, is shown in Fig. 4 (left) for a vehicle starting point equals to  $\boldsymbol{\eta}(0) = (5, 5, 5)^T$  m. The result obtained with the extended guidance law is presented in the same figure, considering a current velocity  $\dot{\boldsymbol{\eta}}_c = (-0.05, -0.1, -0.1)$  m/s. Again, the EGL is able to preserve the ro-

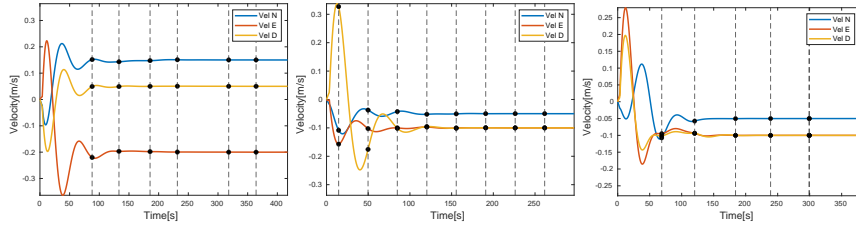


**Fig. 5** Kinematic simulations: estimation of the current velocity in the first (left), second (center), and third (right) simulation scenario.

Parameter value	0.01	22.72	45.43	68.15	90.87	113.58
Real ToA	379.78 s	316.16 s	255.46 s	194.66 s	136.63 s	72.17 s
Estimated ToA	384.11 s	314.12 s	255.66 s	194.67 s	136.64 s	72.17 s

**Table 1** Comparison between estimated time of arrival (Estimated ToA) and simulated time of arrival (Real ToA) in the third scenario for different parameter values.

bustness of the scheme and allows to follow the desired path, as confirmed by the track errors in Fig. 4 (right, top plot) and by the current estimation in Fig. 5 (center).

In the third scenario, we construct the  $C^1$  PH spline interpolating the following seven points:  $\mathbf{p}_0 = (0, 0, 10)^\top$ ,  $\mathbf{p}_1 = (20, 10, 20)^\top$ ,  $\mathbf{p}_2 = (15, 25, 30)^\top$ ,  $\mathbf{p}_3 = (37, 17, 35)^\top$ ,  $\mathbf{p}_4 = (27, 35, 31)^\top$ ,  $\mathbf{p}_5 = (45, 29, 19)^\top$ ,  $\mathbf{p}_6 = (50, 50, 5)^\top$ . The tangents in these points are chosen equal to the tangents obtained with the  $C^2$  cubic spline interpolant. The result is a  $C^1$  PH spline curve composed by six segments, with total length  $L = 153.6724$  m. By considering  $\boldsymbol{\eta}(0) = (5, 5, 15)^\top$  m as starting point of the vehicle, we test the extended version of the guidance law with a drifting current  $\dot{\boldsymbol{\eta}}_c = (-0.05, -0.1, -0.1)$  m/s, see Fig. 4 (center). Fig. 4 (left, bottom plot) shows that the track-errors converge to zero while Fig. 5 (right) confirms that the current estimation converges to the real current. In table 1 we compare the simulated time of arrival of the third simulation scenario with the estimated one. The latter is computed as  $L_r(u)/U_0$ , where  $L_r(u)$  is the length of the portion of the trajectory from the point  $\boldsymbol{\eta}_p(u)$  to the end of the curve. It is clear that, as the vehicle approaches the trajectory, the estimate gets closer to the real data. Finally, we compare the computation time of the arc length using the exact formula available for PH splines with its computation time using the `integral` function of MATLAB. The result confirms that the first computation is 10-11 times faster than the second one.

## 5.2 Dynamic simulatons

We finally validates the performance of the extended guidance law, presenting the results of numerical simulations based on the dynamic model of a real AUV called “Zeno” [14]. The behaviour of a generic marine vehicle is described by the following vectorial equation of 6 components (corresponding to the 6 DoFs),

$$M\dot{\boldsymbol{\nu}} + \mathbf{C}(\boldsymbol{\nu})\boldsymbol{\nu} + \mathbf{D}(\boldsymbol{\nu})\boldsymbol{\nu} + \mathbf{g}(\mathcal{Q}) = \boldsymbol{\tau},$$

together with equation (1) and (2). For a comprehensive description of all the involved quantities see [11]. In the specific case of Zeno, the numerical values of all the dynamic model parameters have been identified in [21]. Any dynamic simulation requires a suitable controller, whose purpose is to compute the vector of thrusts  $\boldsymbol{\tau}$  that the vehicle has to set up in order to follow the kinematic references provided by the guidance law. We choose to design the following model-based controller:

$$\boldsymbol{\tau} = M\mathbf{K}_p\mathbf{e}_p + \mathbf{C}(\boldsymbol{\nu})\boldsymbol{\nu} + \mathbf{D}(\boldsymbol{\nu}_d)\boldsymbol{\nu}_d,$$

where  $\boldsymbol{\nu}_d = ((\mathbf{v}_{rd}^b)^\top, (\boldsymbol{\omega}_d^b)^\top)^\top$  is the vector of references provided by the extended guidance law introduced in Section 4,  $\mathbf{e}_p = \boldsymbol{\nu}_d - \boldsymbol{\nu}$  is the velocity error, and  $\mathbf{K}_p = \text{diag}(20, 0, 0, 0, 10, 10)$  is a  $6 \times 6$  positive definite diagonal matrix containing the tunable parameter for the proportional terms of the controller. Furthermore, we consider to deal with a generic under-actuated vehicle, providing to the simulator a required effort  $\boldsymbol{\tau} = (\tau_x, 0, 0, 0, \tau_p, \tau_r)^\top$  which neglects the terms of sway, heave, and roll. Finally, a saturation on the thrusts has been introduced, based on the electromechanical limits of the real vehicle, In particular, we set a limit of 80N for surge thrust and a limit of  $10\text{N} \cdot \text{m}$  for pitch and yaw torque.

We simulate the behavior of Zeno by considering all the three simulation scenarios. In Fig. 6 it is possible to verify the convergence of the vehicle on the path. The corresponding track errors are reported in Fig. 7. It is remarkable to note that in some cases the cross track error grows again. This effect is connected to the electromechanical limits of the vehicle, which is not able to follow high curvature profiles. However, the error decreases as soon as the curvature gets lower.

## 6 Closure

We presented a robust path following scheme for autonomous vehicles, which allows to handle disturbance effects caused by currents drifting, also suited for under-actuated vehicles. The theoretical validity of the scheme was proved

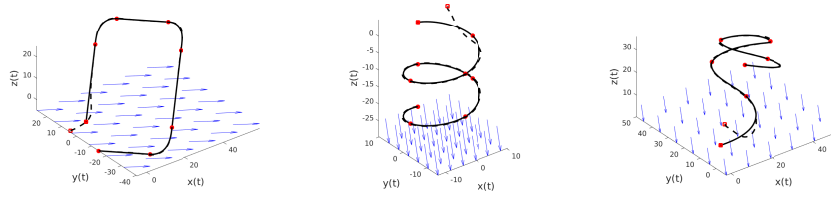


**Fig. 6** Dynamic simulations: the path to be followed (solid line) is shown together with the path of the vehicle (dashed line) for the first (left), the second (center), and the third (right) simulation scenario.

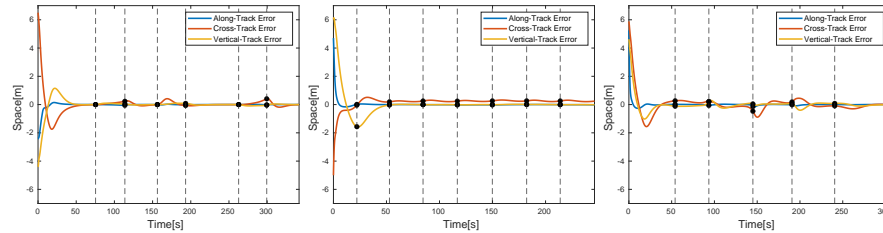


**Fig. 7** Dynamic simulations: track errors for the first (left), the second (center), and the third (right) simulation scenario.

through geometrical and error estimation convergence. Finally, we confirmed the results with simulations based on tangent continuous curvilinear paths obtained by Hermite interpolation with spatial  $C^1$  PH quintic splines, which enable accurate and efficient arrival time estimations. We also tested the guidance law on a classic scenario, considering a 6 DoFs underwater vehicle subject to thrust limitation and decoupled dynamical speed controller. The Zeno AUV model, identified with experimental tests, was used to evaluate the combination of a standard existing controller with the new guidance law under sea current operating condition. The proposed guidance law eases the controller from any integral action and improves convergence by estimating the contribution of the sea current directly into the navigation frame.

## References

1. Souren Asaturyan, Paolo Costantini, and Carla Manni. Local shape-preserving interpolation by space curves. *IMA J. Numer. Anal.*, 21:301–325, 2001.
2. Morten Breivik and Thor I. Fossen. Guidance-Based Path Following for Autonomous Underwater Vehicles. In *Proceedings of OCEANS 2005 MTS/IEEE*, pages 2807–2814, 2005.
3. Morten Breivik and Thor I. Fossen. Guidance Laws for Autonomous Underwater Vehicles. In Alexander V. Inzartsev, editor, *Underwater Vehicles*, chapter 4, pages 51–76. IntechOpen, Rijeka, 2009.

4. Marco Donatelli, Carlotta Giannelli, Duccio Mugnaini, and Alessandra Sestini. Curvature continuous path planning and path finding based on PH splines with tension. *Comput. Aided Design*, 88:14–30, 2017.
5. Gerald Farin. *Curves and Surfaces for Computer Aided Geometric Design*. Academic Press, San Diego, 1997.
6. Rida T. Farouki. *Pythagorean–Hodograph Curves: Algebra and Geometry Inseparable*. Springer, Berlin, 2008.
7. Rida T. Farouki, M. Al Kandari, and T. Sakkalis. Hermite interpolation by rotation-invariant spatial Pythagorean-hodograph curves. *Adv. Comp. Math.*, 17:369–383, 2002.
8. Rida T. Farouki, Carlotta Giannelli, Carla Manni, and Alessandra Sestini. Identification of spatial PH quintic Hermite interpolants with near-optimal shape measures. *Comput. Aided Geom. Design*, 25:274–297, 2008.
9. Rida T. Farouki, Carlotta Giannelli, Duccio Mugnaini, and Alessandra Sestini. Path planning with Pythagorean-hodograph curves for unmanned or autonomous vehicles. *J Aerospace Engineering*, 232:1361–1372, 2018.
10. Rida T. Farouki, Carlotta Giannelli, and Alessandra Sestini. New developments in theory, algorithms, and applications for Pythagorean-hodograph curves. In C. Giannelli and H. Speleers, editors, *Advanced Methods for Geometric Modeling and Numerical Simulation*, pages 127–177. Springer INdAM Series, 2019.
11. Thor I. Fossen. *Guidance and Control of Ocean Vehicles*. John Wiley and Sons, Ltd, 1994.
12. Thor I. Fossen. *Handbook of Marine Craft Hydrodynamics and Motion Control*. John Wiley and Sons, Ltd, 2011.
13. Thor I. Fossen. How to incorporate wind, waves and ocean currents in the marine craft equations of motion. *IFAC Proceedings Volumes*, 45(27):126–131, 2012. 9th IFAC Conference on Manoeuvring and Control of Marine Craft.
14. Jonathan Gelli, Alessia Meschini, Niccolò Monni, Marco Pagliai, Alessandro Ridolfi, Lorenzo Marini, and Benedetto Allotta. Design and Testing of a Compact Autonomous Underwater Vehicle for Archaeological Surveying and Monitoring. In *2018 IEEE/OES Autonomous Underwater Vehicle Workshop (AUV)*, pages 1–6, 2018.
15. Reza Ghabcheloo, Isaac Kaminer, A. Pedro Aguiar, and Antonio Pascoal. A general framework for multiple vehicle time-coordinated path following control. In *2009 American Control Conference*, pages 3071–3076, 2009.
16. Carlotta Giannelli, Duccio Mugnaini, and Alessandra Sestini. Path planning with obstacle avoidance by  $G^1$  PH quintic splines. *Comput. Aided Design*, 75–76:47–60, 2016.
17. Carlotta Giannelli, Duccio Mugnaini, and Alessandra Sestini.  $C^2$  continuous time-dependent feedrate scheduling with configurable kinematic constraints. *Comput. Aided Geom. Design*, 63:78–95, 2018.
18. M. I. Karavelas and P. D. Kaklis. Spatial shape preserving interpolation using  $\nu$ -splines. *Numer. Algor.*, 23:217–250, 2000.
19. Lionel Lapierre and Bruno Jouvencel. Robust nonlinear path-following control of an auv. *Oceanic Engineering, IEEE Journal of*, 33:89–102, 2008.
20. Kikun Park, Sunghyun Sim, and Hyerim Bae. Vessel estimated time of arrival prediction system based on a path-finding algorithm. *Maritime Transport Research*, 2:100012, 2021.
21. Lorenzo Sacco. Identification of zeno auv model parameters. Master’s thesis, Politecnico di Torino, 2020.
22. Alessandra Sestini, L. Landolfi, and Carla Manni. On the approximation order of a space data-dependent PH quintic interpolation scheme. *Comput. Aided Geom. Design*, 30:148–158, 2013.



23. Bruno Siciliano, Lorenzo Sciavicco, Luigi Villani, and Giuseppe Oriolo. *Robotics - Modelling, Planning and Control*. Advanced Textbooks in Control and Signal Processing. Springer, 2nd printing edition, 2008.
24. Andrew Teel, Elena Panteley, and Antonio Loría. Integral Characterizations of Uniform Asymptotic and Exponential Stability with Applications. In *Mathematics of Control, Signals and Systems*, pages 177–201, 2002.
25. Zybnek Šir and Bert Jüttler. Spatial Pythagorean hodograph quintics and the approximation of pipe surfaces. In R. Martin, H. Bez, and M. Sabin, editors, *The Mathematics of Surfaces XI*, pages 364–380, 2005.
26. Huarong Zheng, Rudy R. Negenborn, and Gabriël Lodewijks. Predictive path following with arrival time awareness for waterborne AGVs. *Transportation Research Part C: Emerging Technologies*, 70:214–237, 2016.